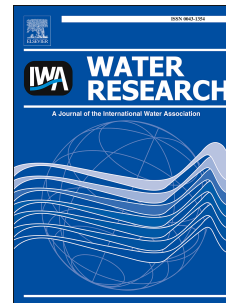


Accepted Manuscript

A mechanistic model for anaerobic phototrophs in domestic wastewater applications:
Photo-anaerobic model (PANM)

D. Puyol, E. Barry, T. Huelsen, D.J. Batstone



PII: S0043-1354(17)30195-1

DOI: [10.1016/j.watres.2017.03.022](https://doi.org/10.1016/j.watres.2017.03.022)

Reference: WR 12759

To appear in: *Water Research*

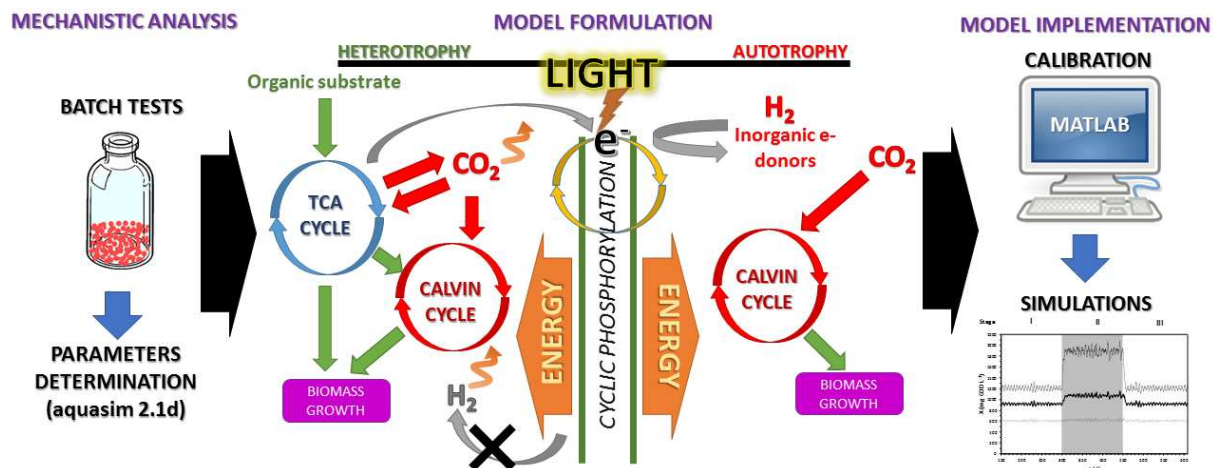
Received Date: 9 December 2016

Revised Date: 7 March 2017

Accepted Date: 8 March 2017

Please cite this article as: Puyol, D., Barry, E., Huelsen, T., Batstone, D.J., A mechanistic model for anaerobic phototrophs in domestic wastewater applications: Photo-anaerobic model (PANM), *Water Research* (2017), doi: 10.1016/j.watres.2017.03.022.

This is a PDF file of an unedited manuscript that has been accepted for publication. As a service to our customers we are providing this early version of the manuscript. The manuscript will undergo copyediting, typesetting, and review of the resulting proof before it is published in its final form. Please note that during the production process errors may be discovered which could affect the content, and all legal disclaimers that apply to the journal pertain.



1 **A mechanistic model for anaerobic phototrophs in**
2 **domestic wastewater applications: Photo-Anaerobic Model**
3 **(PAnM)**

4 *D. PUYOL^{a,b,c,*}, E. BARRY^{a,b}, T. HUELSEN^{a,b}, D.J. BATSTONE^{a,b}.*

5 *a Advanced Water Management Centre, Gehrmann Building, The University of*
6 *Queensland, Brisbane, Queensland 4072, Australia*

7 *b CRC for Water Sensitive Cities, PO Box 8000, Clayton, Victoria, 3800, Australia*

8 *c Group of Chemical and Environmental Engineering (GIQA), University Rey Juan*
9 *Carlos, 28933 Mostoles, Madrid, Spain*

10 * Corresponding author information: daniel.puyol@urjc.es. *Departamental Building I,*
11 *Room 234. Mostoles Campus. University Rey Juan Carlos. C/ Tulipán, S/n, 28933 -*
12 *Mostoles - Madrid – Spain. Tel: +34 914888095 (ext. 8095), Fax: +34 914887086*

13

14 **ABSTRACT**

15 Purple phototrophic bacteria (PPB) have been recently proposed as a key potential
16 mechanism for accumulative biotechnologies for wastewater treatment with total nutrient
17 recovery, low greenhouse gas emissions, and a neutral to positive energy balance. Purple
18 phototrophic bacteria have a complex metabolism which can be regulated for process
19 control and optimization. Since microbial processes governing PPB metabolism differ from
20 traditional processes used for wastewater treatment (e.g., aerobic and anaerobic functional
21 groups in ASM and ADM1), a model basis has to be developed to be used as a framework
22 for further detailed modelling under specific situations. This work presents a mixed
23 population phototrophic model for domestic wastewater treatment in anaerobic conditions.
24 The model includes photoheterotrophy, which is divided into acetate consumption and other
25 organics consumption, chemoheterotrophy (including simplified fermentation and anaerobic
26 oxidation) and photoautotrophy (using hydrogen as an electron donor), as microbial
27 processes, as well as hydrolysis and biomass decay as biochemical processes, and is
28 single-biomass based. The main processes have been evaluated through targeted batch
29 experiments, and the key kinetic and stoichiometric parameters have been determined. The
30 process was assessed by analyzing a continuous reactor simulation scenario within a long-
31 term wastewater treatment system in a photo-anaerobic membrane bioreactor.

32 *Key words: Phototrophic bacteria, resource recovery, mechanistic modelling, Partition-*
33 *Release-Recovery*

34 **NOMENCLATURE**

35 ADM1 - IWA Anaerobic Digestion Model #1

36 ASM – IWA Activated Sludge Models

37 $f_{ac,ch}$ – Stoichiometry of acetate production in chemoheterotrophy (mgCOD mgCOD⁻¹)38 $f_{C,B}$ – Carbon content of PPB (molC mgCOD⁻¹)39 $f_{C,si}$ – Carbon content of soluble inert (molC mgCOD⁻¹)40 $f_{C,xi}$ – Carbon content of particulate inert (molC mgCOD⁻¹)41 $f_{C,xs}$ – Carbon content of biodegradable particulate (molC mgCOD⁻¹)42 $f_{h2,a}$ – Stoichiometry of hydrogen consumption in autotrophy (mgCOD molC⁻¹)43 $f_{h2,ch}$ – Stoichiometry of hydrogen production in chemoheterotrophy (mgCOD mgCOD⁻¹)44 $f_{h2,xs}$ – Stoichiometry of hydrogen production in hydrolysis (mgCOD mgCOD⁻¹)45 $f_{IC,a}$ – Stoichiometry of inorganic carbon consumption in autotrophy (molC molC⁻¹)46 $f_{IC,ph,ac}$ – Stoichiometry of inorganic carbon produced from acetate in photoheterotrophy
47 (molC mgCOD⁻¹)48 $f_{IC,ph,ss}$ – Stoichiometry of inorganic carbon produced from soluble fraction of substrate but
49 acetate in photoheterotrophy (molC mgCOD⁻¹)50 $f_{IC,xs}$ – Stoichiometry of inorganic carbon production in hydrolysis (molC mgCOD⁻¹)51 $f_{IN,xs}$ – Stoichiometry of ammonia production in hydrolysis (mgN mgCOD⁻¹)52 $f_{IP,xs}$ – Stoichiometry of phosphate production in hydrolysis (mgP mgCOD⁻¹)53 $f_{N,B}$ – Nitrogen content of PPB (mgN mgCOD⁻¹)54 $f_{N,si}$ – Nitrogen content of soluble inert (mgN mgCOD⁻¹)55 $f_{N,xi}$ – Nitrogen content of particulate inert (mgN mgCOD⁻¹)56 $f_{N,xs}$ – Nitrogen content of biodegradable particulate (mgN mgCOD⁻¹)57 $f_{P,B}$ – Phosphorus content of PPB (mgP mgCOD⁻¹)58 $f_{P,si}$ – Phosphorus content of soluble inert (mgP mgCOD⁻¹)59 $f_{P,xi}$ – Phosphorus content of particulate inert (mgP mgCOD⁻¹)60 $f_{P,xs}$ – Phosphorus content of biodegradable particulate (mgP mgCOD⁻¹)

- 61 $f_{SAc,xs}$ – Stoichiometry of acetate production in hydrolysis (mgCOD mgCOD⁻¹)
- 62 $f_{si,xs}$ – Stoichiometry of soluble inert production in hydrolysis (mgCOD mgCOD⁻¹)
- 63 $f_{ss,xs}$ – Stoichiometry of soluble substrate production but acetate in hydrolysis (mgCOD
- 64 mgCOD⁻¹)
- 65 $f_{xi,xs}$ – Stoichiometry of particulate inert production in hydrolysis (mgCOD mgCOD⁻¹)
- 66 HA – Hydrogenogenic activity (mgCOD_{h2} L_{liq}⁻¹ d⁻¹)
- 67 HA_{max} – Maximum hydrogenogenic activity (mgCOD_{h2} L_{liq}⁻¹ d⁻¹)
- 68 HRT – Hydraulic retention time (h)
- 69 I_{FA} – Limiting factor for free ammonia inhibition
- 70 I_E – Limiting factor for light limitation
- 71 I_{IN} – Limiting factor for nitrogen limitation
- 72 I_{IP} – Limiting factor for phosphorus limitation
- 73 k_{dec} – Biomass decay first order constant (d⁻¹)
- 74 k_{hyd} – Hydrolysis first order constant (d⁻¹)
- 75 $K_{i,FA}$ – Inhibitory constant for free ammonia (mgN L⁻¹)
- 76 $k_{M,ac}$ – Specific uptake rate for acetate in photoheterotrophy (mgCOD mgCOD⁻¹ d⁻¹)
- 77 $k_{M,but}$ – Specific uptake rate for butyrate in photoheterotrophy (mgCOD mgCOD⁻¹ d⁻¹)
- 78 $k_{M,ch}$ – Specific uptake rate in chemoheterotrophy (mgCOD mgCOD⁻¹ d⁻¹)
- 79 $k_{M,et}$ – Specific uptake rate for ethanol in photoheterotrophy (mgCOD mgCOD⁻¹ d⁻¹)
- 80 $k_{M,ic}$ – Specific uptake rate of IC in autotrophy (molC mgCOD⁻¹ d⁻¹)
- 81 $k_{M,ph}$ – Specific uptake rate in photoheterotrophy (mgCOD mgCOD⁻¹ d⁻¹)
- 82 $k_{M,prop}$ – Specific uptake rate of propionate in photoheterotrophy (mgCOD mgCOD⁻¹ d⁻¹)
- 83 $K_{S,ac}$ – Saturation constant for acetate in photoheterotrophy (mgCOD L⁻¹)
- 84 $K_{S,but}$ – Saturation constant for butyrate in photoheterotrophy (mgCOD L⁻¹)
- 85 $K_{S,E}$ – Saturation constant for light intensity (W m⁻²)
- 86 $K_{S,et}$ – Saturation constant for ethanol in photoheterotrophy (mgCOD L⁻¹)
- 87 $K_{S,h2}$ – Saturation constant for H₂ consumption in autotrophy (mgCOD L⁻¹)
- 88 $K_{S,ic}$ – Saturation constant for inorganic carbon in autotrophy (molC L⁻¹)

- 89 $K_{S,prop}$ - Saturation constant for propionate in photoheterotrophy (mgCOD L⁻¹)
- 90 $K_{S,s}$ - Saturation constant for soluble substrate but acetate in photoheterotrophy (mgCOD L⁻¹)
- 91 K_{Sin} - Saturation constant for inorganic nitrogen assimilation (mgN L⁻¹)
- 92 K_{Sip} - Saturation constant for inorganic phosphorus assimilation (mgP L⁻¹)
- 93 S_{ac} - Concentration of acetate (mgCOD L⁻¹)
- 94 SCOD - Soluble chemical oxygen demand (mgCOD L⁻¹)
- 95 S_{h2} - Concentration of hydrogen as COD (mgCOD L⁻¹)
- 96 S_I - Concentration of soluble inerts (mgCOD L⁻¹)
- 97 S_{IC} - Concentration of inorganic carbon (molC L⁻¹)
- 98 S_{IN} - Concentration of inorganic nitrogen as ammonia (mgN L⁻¹)
- 99 S_{IP} - Concentration of inorganic phosphorus as phosphate (mgP L⁻¹)
- 100 SPA - Specific phototrophic activity (mgCOD mgCOD⁻¹ d⁻¹)
- 101 SRT - Solids retention time (d⁻¹)
- 102 S_s - Concentration of biodegradable soluble fraction but acetate (mgCOD L⁻¹)
- 103 TCOD - Total chemical oxygen demand (mgCOD L⁻¹)
- 104 TIC - Total inorganic carbon (molC L⁻¹)
- 105 TKN - Total Kjeldahl Nitrogen (mgN L⁻¹)
- 106 TP - Total phosphorus (mgP L⁻¹)
- 107 TSS - Total suspended solids (mg L⁻¹)
- 108 VFA - Volatile fatty acids (mgCOD L⁻¹)
- 109 VLR - Volumetric loading rate (mgCOD L⁻¹ d⁻¹)
- 110 VSS - Volatile suspended solids (mg L⁻¹)
- 111 X_I - Concentration of particulate inerts (mgCOD L⁻¹)
- 112 X_{PB} - Concentration of PPB biomass (mgCOD L⁻¹)
- 113 X_S - Concentration of organic biodegradable particulate (mgCOD L⁻¹)
- 114 Y_{ac} - Biomass yield on acetate in photoheterotrophy (mgCOD mgCOD⁻¹)
- 115 Y_{but} - Biomass yield on butyrate in photoheterotrophy (mgCOD mgCOD⁻¹)
- 116 Y_{et} - Biomass yield on ethanol in photoheterotrophy (mgCOD mgCOD⁻¹)

- 117 $Y_{PB,a}$ - Biomass yield in autotrophy (mgCOD molC⁻¹)
- 118 $Y_{PB,ch}$ - Biomass yield in chemoheterotrophy (mgCOD mgCOD⁻¹)
- 119 $Y_{PB,ph}$ - Biomass yield in photoheterotrophy (mgCOD mgCOD⁻¹)
- 120 Y_{prop} - Biomass yield on propionate in photoheterotrophy (mgCOD mgCOD⁻¹)

ACCEPTED MANUSCRIPT

121 **1 INTRODUCTION**

122 Wastewater treatment is shifting focus to include the capture and recovery of organics and
123 nutrients. This requires novel technological approaches. A key approach is the use of fast
124 growing organisms to concentrate energy, nutrients, and trace compounds into the solid
125 phase, and hence substantially reduce reactive removal of nitrogen and organics while
126 enabling phosphorous recovery. One option is high-rate activated sludge, which can achieve
127 40% nitrogen removal in the primary stage through adsorption and assimilation (Jetten et al.
128 1997). Algae can also be used to partition to the solid phase, but a simultaneous
129 heterotrophic and photosynthetic mode is generally enabled by bacterial-algal associations
130 that reduce organic substrate consumption efficiency (Muñoz and Guieysse 2006). Purple
131 phototrophic bacteria (PPB) present a new partitioning approach, which has been shown to
132 completely remove nitrogen to discharge limits when sufficient organic carbon is present
133 without the need for pure cultures, and using infra-red (IR)light only as a driver for growth
134 (Hülsemann et al. 2014).

135 PPB grow phototrophically rather than photosynthetically, and do not use water as an
136 electron donor to produce oxygen and organics. They are among the most metabolically
137 versatile organisms on earth (Hunter et al. 2008). They grow heterotrophically using a wide
138 range of organic compounds, both in presence and absence of light (photoheterotrophy and
139 chemoheterotrophy) (Hunter et al. 2008). However, they can also grow autotrophically by
140 using infrared light as the energy driver for CO₂ fixation, and with inorganic electron donors
141 such as H₂, Fe²⁺, S²⁻ or S₂O₃²⁻ (cyclic anoxygenic photosynthesis) (Overmann and Garcia-
142 Pichel 1998). Although they can grow in the presence of oxygen, they are extremely
143 effective in anaerobic photoheterotrophic conditions (Gordon and McKinlay 2014, McKinlay
144 and Harwood 2010). Their ability to recycle electrons during the cyclic anoxygenic
145 photosynthesis gives them the ability to harvest and retain electrons, as well as a high
146 energetic efficiency. This entails a much higher biomass yield on organic substrates than

147 traditional aerobic biomass (near 1 vs 0.6 gCOD dCOD⁻¹) (Hülßen et al., 2014). They can
148 even accumulate electrons in the form of reduced cofactors which enable the disposal of
149 electrons. This can be done through two main strategies: (i) ATP-driven hydrogen production
150 by ferredoxin oxidation in the hydrogenase/nitrogenase system at the end of the electron
151 transport chain (ETC), and (ii) the increase of assimilative growth by re-fixation of CO₂ via
152 the Calvin Cycle produced during heterotrophic metabolism (McKinlay and Harwood 2010).
153 These metabolic features give them the possibility of growing and out-competing other
154 heterotrophic microorganisms where light is present, including in low to medium strength
155 wastewater systems with short hydraulic retention times (HRT) (Hülßen et al. 2014).

156 PPB have a number of additional metabolic functions useful in wastewater treatment
157 systems. They are able to accumulate polymers such as poly-phosphate (poly-P) (Liang et
158 al. 2010), polysaccharides (Klein et al. 1991), poly-β hydroxybutyrate (PHB) (Melnicki et al.
159 2009) and other poly-3(hydroxyalkanoates) (PHA) (Brandl et al. 1991). Under an excess of
160 organics and available energy, and in the absence of mineral nitrogen, they generate
161 hydrogen and fix nitrogen as ammonia (Basak and Das 2007).

162 PPB have been assessed for wastewater treatment, particularly for processing swine (Kim et
163 al. 2004), latex rubber-sheet (Kantachote et al. 2005), tofu (Zhu et al. 1999), and sugar
164 refinery wastewaters (Yetis et al. 2000). However, most of these studies were focused on
165 hydrogen production rather than organics removal or nutrient recovery (Fang et al. 2005,
166 Lee et al. 2010, Tao et al. 2008). They have also been applied to domestic wastewater
167 (DWW) in batch and continuous operation to remove nitrogen to discharge limits (Hülßen et
168 al. 2014). This process enables a single-step treatment of wastewater with HRT and effluent
169 qualities similar to those of activated sludge processes without destroying nitrogen and
170 phosphorus.

171 Modelling is used to design, benchmark, and analyze wastewater treatment systems, with
172 the IWA Activate Sludge Model (ASM) family models being the most widely used for
173 conventional activated sludge processes (Henze et al. 2000). The IWA anaerobic digestion

174 model no. 1 (ADM-1) is the analogous model for domestic and industrial anaerobic systems
175 (Batstone et al. 2002). The IWA Models, and wastewater modelling in general has generally
176 applied first order hydrolysis for solids transformation (including decay), Monod kinetic
177 function for uptake kinetics and inverse Monod kinetic function (non-competitive) for
178 inhibition functions, with a COD basis for organics and molar basis for inorganic compounds.
179 Development of new technologies such as PPB requires development of a similar
180 mechanistic model to allow process control, design, and system analysis in upscaled
181 applications.

182 There are complex metabolic models based on PPB metabolism primarily focused on the
183 electron transport chain (Golomysova et al. 2010, Klamt et al. 2002). Due to their complexity,
184 these models are motivated more by a need for a mechanistic understanding of the
185 underlying process rather than field applications. These models are therefore unsuitable for
186 a wastewater model. In particular, they include components which can't be measured
187 readily, making validation difficult. They also lack capability outside the core application area.
188 There has also been work done on modelling PPB to describe hydrogen production (Eroglu
189 2008, Gadhamshetty et al. 2008, Obeid et al. 2009). In contrast, due to the domestic
190 wastewater matrix, the key growth modes are photoheterotrophy (principal) as well as
191 chemoheterotrophy and photoautotrophy. Biochemical processes relevant to complex
192 substrates such as solids hydrolysis and biomass decay must be considered as well.
193 Therefore, this work aims to propose a mechanistic model for mixed culture PPB as a
194 partition agent in DWW treatment with adaptability to treatment of industrial wastewaters.

195 2 Materials and Methods

196 2.1 Model Description

197 The model was developed to be unit-compatible with the IWA ASM and ADM series
198 (Batstone et al. 2002, Henze et al. 2000). Therefore, units of mgCOD L^{-1} (or gCOD m^{-3}) for

199 both soluble and particulate organics were chosen. Nutrient units are in mgN L^{-1} and mgP L^{-1} , respectively, with inorganic carbon (IC, HCO_3^-) in molC L^{-1} .

201 Monod kinetics is uniformly applied for biological growth processes, with first order kinetics
202 for hydrolysis and decay. Monod or non-competitive inhibition has been applied for limiting or
203 inhibitory expressions respectively. Due to a lack of functional differentiation within the PPB
204 clade, and limited evidence to the contrary, only one biomass component has been selected
205 (PPB) (Hülsem et al., 2015b). Other biological groups present in ASM and ADM1 models
206 (e.g., hydrogen utilizing methanogens, denitrifiers or fermentative bacteria) could be readily
207 included. As in the ASM/ADM models S_i is used for soluble compounds, and X_i for
208 particulate compounds, where subscript i denotes the compound.

209 The model does not currently include poly-P or other polymer accumulation, since this
210 occurs mainly in static (not growing) mode, where PPB can derive energy to stock resources
211 for further usage in growing conditions (Hiraishi et al. 1991, Liang et al. 2010). Likewise,
212 nitrification/denitrification processes are not included, since they can only occur in, or in
213 combination with aerobic conditions where ammonia can be oxidized to nitrite or nitrate.
214 Therefore, N and P are removed by assimilative growth only.

215 In the presence of organic substrates and IR light, photoheterotrophy through the tri-
216 carboxylic acid (TCA) cycle is assumed to dominate. Two major mechanisms of electron
217 disposal by PPB are considered. Firstly, the production of CO_2 (S_{IC}) is a key feature of PPB
218 biomass under growth conditions (McKinlay and Harwood 2010) and is important for closing
219 the C balance. The oxidation state of the organic compound determines if the biomass fixes
220 CO_2 for substrate uptake and electron balance (in the case of reduced substrates such as
221 propionate, butyrate or valerate), or the uptake produces CO_2 (in the case of oxidized
222 substrates such as acetate or succinate) (McKinlay and Harwood 2011). In the latter case,
223 the biomass disposes of excess of electrons by re-fixing the CO_2 produced in the TCA cycle.
224 As a consequence, there is usually limited consumption or production of CO_2 in domestic
225 wastewater. A theoretical explanation of this mechanism is explained in Supplementary

226 Information (SI). The other major mechanism of electron disposal by PPB is H₂ production
227 via the nitrogenase complex. In static growth mode, the PPB biomass is able to use the
228 excess of electrons for redox balance at the end of the ETC. The ferredoxin complex is the
229 carrier for this process, but the biomass needs energy in the form of ATP (Golomysova et al.
230 2010). However, this process is inhibited in presence of NH₄⁺, a strong inhibitor of the
231 nitrogenase activity (Rodionov et al. 1986). Indeed, H₂ production is inhibited in a DWW fed
232 situation due to (i) presence of ammonium and (ii) disposing of electrons by CO₂ re-fixation
233 which promotes growth (see SI for more details). Therefore, it can be deduced that CO₂
234 production and re-fixation into the Calvin Cycle is the major electron sink in PPB metabolism.
235 In the absence of organic substrates, autotrophic growth is the sole growth mode, using
236 reduced inorganic compounds other than water as electron donor (anoxygenic
237 photosynthesis). In the interest of model simplification and considering domestic wastewater
238 contains generally low sulfur levels, the sulfur cycle has been omitted. It is however possible
239 to add sulfate reduction into the model with subsequent sulfide utilization as an electron
240 donor for autotrophic PPB growth. This would require the addition of another biomass
241 component (PPB cannot perform sulfate reduction). PPB can perform chemoheterotrophy at
242 a lower rate, providing H₂ (S_{h2}) for photoautotrophy (Golomysova et al. 2010).

243 Transforming these mechanisms to a model enables the following key processes (Figure 1):

- 244 (i) *Photoheterotrophy on acetate (S_{ac}) (acetate uptake)*: This involves acetate
245 assimilation by PPB in the presence of infra-red radiation. Acetate is represented
246 as a separate state due to differences observed during batch tests. Due to an
247 imbalance in substrate-biomass carbon oxidation state, this process results in
248 production of CO₂.
- 249 (ii) *Photoheterotrophy on other organics (S_s) (photoheterotrophic uptake)*: These
250 include all soluble organics that PPB can assimilate for growth in the presence of
251 infra-red radiation. Compounds include VFAs excluding acetate, alcohols, and

- 252 some sugars. These have been lumped into a single soluble substrate. Similar to
253 (i) this results in the uptake of CO_2 .
- 254 (iii) *Chemoheterotrophy (chemoheterotrophic uptake)*: This process involves the
255 assimilative consumption of any organic in dark conditions that can be
256 metabolized through either fermentation or anaerobic oxidation processes. All
257 these processes have been joined as one process for a sake of simplicity. This
258 process involves H_2 and acetate as end products. Acetate is not further oxidized
259 through chemoheterotrophy due to a lack or very limited terminal electron
260 acceptors such as Fe(III) and sulfate (Finneran et al. 2003).
- 261 (iv) *Photoautotrophy (autotrophic uptake)*: This process involves assimilative CO_2
262 fixation by PPB in the presence of infra-red radiation using H_2 as the electron
263 donor. Other electron donors such as Fe^{2+} , S^{2-} and S_2O_3^- have been omitted but
264 could be included.
- 265 (v) *PPB cell death (decay)*: This process involves the deactivation of PPB by cell
266 death. Ammonium, phosphate and inorganic carbon are released and the
267 biomass is converted into biodegradable organic particulates (X_S) and particulate
268 inerts (X_I).
- 269 (vi) *Hydrolysis and particulate fermentation (hydrolysis)*: The decomposition of
270 biodegradable particulates into organics (S_{ac} and S_S), ammonium, phosphate,
271 hydrogen and inorganic carbon is addressed as a sole process for simplicity.
272 Both soluble and particulate inerts are also products of this process. A
273 breakdown of particulate fermentation could be incorporated into the model e.g.
274 for processes with long solids retention times (SRT).

275 The model is presented in Petersen matrix notation in Table 1. Kinetic parameters were
276 generally obtained from the batch experiments, or from the literature in specific cases as
277 described below. The saturation constant for hydrogen consumption by photoautotrophic
278 process (K_{S,h_2}), light limitation ($K_{S,E}$) and inhibition by free ammonia ($K_{i,FA}$) were set arbitrarily

279 low since affinity is high (Chen et al. 2008, Uyar et al. 2007). Competitive inhibition between
280 S_{ac} and S_S in photoheterotrophic metabolism has been included by using a parameter-less
281 switch function as in the case of the ADM1. A detailed experimental evidence for such a
282 function is presented in Supplementary Information (S9). Stoichiometry was determined by
283 both theoretical calculations from literature, and experimentally. The model is balanced over
284 COD, C, N and P. Carbonates (S_{IC}), inorganic nitrogen (S_{IN}) and phosphates (S_{IP}) have been
285 used for closing C, N and P balances, respectively.

286 A basic ideal activity pH model has been included as for the ADM1 (Batstone *et al*, 2002),
287 with inclusion of the phosphate ($H_2PO_4^-/HPO_4^{2-}$) acid-base pair, and with no ion pairing. This
288 provides essential representation for domestic wastewater strength, but should be extended
289 to the strong acids and bases (H_3PO_4 , PO_4^{-3} , CO_3^{2-}) where precipitation occurs, pH
290 extremes, or higher strength is important, or where plant-wide modelling is applied as
291 discussed in Batstone *et al.*, (2012). Acid-base equations are formulated into the charge
292 balance, which is solved for the single unknown of hydrogen ion (S_H) using the Matlab
293 command `fzero`. Temperature is currently fixed to 25°C, but can be incorporated via the
294 van't Hoff equations as for Batstone *et al.*, (2002). Background cations (S_{cat}) was set at
295 0.003M to account for strong cations coupled with input bicarbonate (setting input pH to 6),
296 but an alternative implementation where it was linked to bicarbonate was also evaluated.
297 Acetate (S_{ac}) was added as glacial acetic acid. If sodium acetate were added instead,
298 additional cations (S_{cat}) would need to be included. Non-VFA organics (S_S) was given an
299 acidic fraction of 50%, assuming it to be propionic acid, with the remainder being alcohols
300 and sugars.

301 Additional details concerning model development and implementation can be found in the
302 supplementary information (SI) and codes can be found on the UQ repository
303 (<http://espace.library.uq.edu.au/view/UQ:412280>). SI1 includes the description of model
304 components, full kinetic parameters and stoichiometric coefficients. The determination and

305 calibration of stoichiometry is included in SI2, and SI4 contains the full list of model
306 equations.

307 *Model integration with ASM-family models and ADM1*

308 Soluble organic compounds can be readily transformed into ASM organic substrate (where
309 $S_{s_ASM} = S_{ac} + S_{s_PAnM}$). Organic particulates in the PAnM correspond to the X_s in the
310 ASM. For the ADM1 integration, an interface can be used following Nopens et al. (2009),
311 with units generally being compatible. Mechanisms for organic biodegradable particulates to
312 engage with the ADM1 can be approximated as follows: $X_{PPB} \rightarrow (aX_{ch} + bX_{li} + cX_{pr} + dX_i)$,
313 where a, b, c and d are the carbohydrate, lipid, protein and inerts content of the PPB
314 biomass as for Nopens *et al.*, (2009). As PPB have different composition of other
315 feedstocks, it is necessary to identify a, b, c and d parameters through nitrogen content and
316 COD:mass ratios as done in Nopens *et al.*, (2009). Generally, N content of PPB biomass is
317 significantly higher than typical waste sludge (Hülßen et al., 2014), and this increases c. Both
318 soluble and particulate inerts have the same meaning than their respective counterparts in
319 the ASM and ADM1 models.

320 Inorganic nitrogen can be directly transformed into ASM inorganic nitrogen since S_{IN_PAnM}
321 $= S_{nh} + S_{no}$ (in mgN L⁻¹). Inorganic nitrogen in the PAnM (ammonium) has the same meaning
322 that in the ADM1. However, total nitrogen can be integrated into ADM1 parameters by
323 following the lump–delump approach of the Copp interface (Copp et al., 2003). Inorganic
324 phosphorus in the PAnM has the same meaning that S_{IP} in the ADM1 and S_{PO4} in the
325 ASM2d. The inorganic carbon in the PAnM has the same meaning as in the ADM1. Alkalinity
326 from ASM models can be transformed into S_{IC} as in the case of the ASM1/ADM1 interface
327 (Nopens et al., 2009).

328 2.2 Batch Experiments

329 Batch experiments were done to identify parameters based on the developed model. The
330 inoculum was sourced from a lab-scale continuous photo-anaerobic membrane bioreactor

331 (PAnMBR) described by (Hülßen et al. 2016b) operated over 300 d. Domestic wastewater
332 was collected from the Taringa wastewater lift station (Brisbane, Australia) with an average
333 strength of 572 mgCOD L⁻¹ and soluble COD of 241 mgCOD L⁻¹, 63 mgN L⁻¹, and 9 mgP L⁻¹.

334 Where wastewater was not the medium, synthetic Ormerod medium was used at pH 7.5 as
335 described previously (Hülßen et al. 2014).

336 *Metabolic growth batch tests:* All batch tests were done in 100mL working volumes (160 mL
337 serum flasks) in triplicate, inoculated from the PAnMBR reactor. The headspace was flushed
338 with N₂ and experiments were carried out at 20 °C in an orbital shaker at 150 rpm (Edwards
339 Instrument Company). The array of flasks was irradiated with 150W lamps using UV-VIS
340 absorbing foil as described elsewhere (Hülßen et al. 2014). All experiments were
341 accompanied by blank samples with no substrate, and by positive and negative controls
342 where necessary. A summary is provided in Table 2.

343 *Hydrolysis and biomass decay:* The inoculum (0.5 L) was collected as per the above method
344 (2.1 g VSS L⁻¹). The biomass was centrifuged in 50 mL Falcon tubes and the pellet
345 resuspended again in NaCl 0.2 M three times. Biomass was then placed in 0.5 L of NaCl 0.2
346 M and was divided into two 0.25 L Schott bottles, which were subsequently flushed with N₂
347 and magnetically stirred at 200 rpm. The bottles were operated for 30 d.

348 One of the bottles was covered with aluminum foil to avoid phototrophic activity, and was
349 used for the hydrolysis analysis. Liquid sampling was performed twice a week to analyze
350 volatile fatty acids (VFAs), NH₄-N, PO₄-P, total inorganic carbon (TIC) and pH. Headspace
351 was analyzed for CH₄, H₂ and CO₂. TSS/VSS, TKN and TP was analyzed every 7 d.

352 The other bottle was illuminated as indicated above without feed, and biomass samples
353 were taken every 7 d to assess activity (determining decay coefficient). Activity tests were
354 done as above with 100 mgCOD L⁻¹ of acetate and 10 mg NH₄-N L⁻¹.

355 *Calculation of Specific Phototrophic Activities (SPA).* Non-linear parameter estimation is
356 generally used to determine parameters as described in 2.4.2, but specific phototrophic

357 activity was also determined by linear regression of substrate concentration over a minimum
358 of four points through the region of maximum consumption divided by biomass
359 concentration.

360 2.3 Analytical methods

361 Total COD (TCOD) and soluble COD (SCOD) were determined by COD cell tests (Merck,
362 1.14541.0001, Darmstadt, Germany). Dissolved $\text{NH}_4\text{-N}$, $\text{NO}_2\text{-N}$ and $\text{PO}_4\text{-P}$ were determined
363 by a QuikChem8000 Flow Injection Analyzer (FIA) (Hach Company, Loveland, USA).
364 Temperature and pH were measured using an Oakton pH 11 Series (Vernon Hill, IL, USA).
365 TSS and VSS were determined by filtration according to standard methods where TSS were
366 calculated after drying the sample in an oven at 105 ± 2 °C and VSS were calculated after
367 burning it in a furnace at 550 ± 5 °C (APHA. 1998). Illuminance (W m^{-2}) was measured with
368 an IR light sensor (PAS PortTM, Roseville, CA, USA). VFA samples were analyzed by gas
369 chromatography (Agilent Technologies 7890A GC System, Santa Clara, CA, USA) equipped
370 with a flame ionization detector (GC/FID) and a polar capillary column (DB-FFAP). Gas
371 samples were analyzed by GC (2014 Shimadzu, Kyoto, Japan) with thermal coupled
372 detector (TCD) (Tait et al. 2009). TKN and TP were determined using sulfuric acid,
373 potassium sulfate and copper sulfate catalyst in a block digester (Lachat BD-46, Hach
374 Company, Loveland, CO, USA) (Patton and Truitt 1992). TIC was analyzed by using a total
375 organic carbon (TOC) analyzer (Shimadzu TOC-L CSH TOC Analyzer with TNM-L TN unit)
376 coupled to a near infrared detector (NIRD) for measuring the CO_2 . All soluble constituents
377 were determined after filtering with a $0.45 \mu\text{m}$ membrane filter (Millipore, Millex[®]-HP, Merck
378 Group, Darmstadt, Germany).

379 2.4 Data analysis

380 2.4.1 Data handling

381 Biomass concentration was calculated in g VSS L⁻¹, and it was further transformed into COD
382 by using the COD relationship calculated from the biomass equation CH_{1.8}O_{0.38}N_{0.18}
383 (McKinlay and Harwood 2010) (1 g biomass expressed as VSS = 1.78 gCOD).

384 Biomass yields (Y) were calculated accounting for the initial and final biomass concentration
385 (in g VSS L⁻¹) based on substrate consumption. Biomass concentration was further
386 transformed into COD and then yields are expressed as mgCOD_{biomass} mgCOD⁻¹.

387 2.4.2 Statistical analyses and uncertainty assessment

388 Good measurement practice was applied to minimize uncertainty. Where measurements
389 were outside the calibration range, these were repeated by diluting the sample. Internal or
390 external standards were used for all measurements. Calibration of equipment was performed
391 at least once per week.

392 All parameters were estimated from triplicate batch/measurements by minimization of
393 residual sum of squares (J=RSS). Parameter uncertainty was determined using two-tailed *t*-
394 tests calculated from standard error in parameter value, obtained from the Fisher information
395 matrix. Where parameter optimization problems involve multiple parameters (k_M , K_S),
396 parameter uncertainty surface (J=J_{crit}) has also been assessed as described in (Batstone et
397 al. 2003) . Confidence intervals (at 95%) were also calculated based on two-tailed *t*-tests
398 from parameter standard error, as above, and used for statistical representative
399 comparisons. Error bars in experimental data represent 95% confidence intervals in mean
400 based on a two-tailed *t*-test (5% significance threshold). Uncertainty of the slope for the
401 analysis of SPA was determined by error in slope from linear regression in Microsoft Excel
402 2013 (using the Regression tool in the Data Analysis toolpack). Standard error in slope was
403 subsequently converted into 95% confidence interval (two-tailed *t*-test). All statistical
404 analyses were done with a 5% significance threshold.

405 2.5 Simulation of a continuous PAnMBR

406 The resulting kinetic expressions were used in the development of a continuous PAnMBR
407 model. As previously demonstrated, the concentration of the bioavailable SCOD in medium
408 strength domestic wastewater is insufficient for the system to achieve total nitrogen and total
409 phosphorous discharge limits (Hülse et al. 2016b). To achieve full removal, additional
410 SCOD is required.

411 The goals of the simulation were the following: a) to highlight the requirement of additional
412 SCOD to achieve total nutrient removal, and b) to demonstrate that the inclusion of a primary
413 clarifier can lead to an organic sludge enriched in PPB biomass. Dynamic influent data was
414 simulated according to the influent generator model developed by Gernaey et al. (2011), and
415 adapted to the typical concentrations of primary influent reported by Hülse et al., 2014.
416 Based on the average influent characteristics and an HRT of 12 h, volumetric loading rate
417 (VLR) of $1400 \pm 12 \text{ mgCOD L}^{-1} \text{ d}^{-1}$ and a solid retention time (SRT) of 3 d, a reactor volume
418 of 70 m^3 was applied. An ideal primary clarifier was included, with a solids removal efficiency
419 of $60\% \pm 3\%$ (Tchobanoglous et al., 2002).

420 Simulation and subsequent data processing were done in Matlab (MATLAB R2015a, The
421 MathWorks Inc., Natick, MA). As the system of equations is stiff, the system of ordinary
422 differential equations was solved by ODE15s. The case was simulated for 609 days with 3
423 stages of differing SCOD concentrations. The dynamic influent after settling was applied
424 directly during Stage I until day 300. During Stage II (days 300-450), acetate was added to
425 the optimum COD/N/P ratio of 100/7.1/1.8 (optimum ratio calculation reported in SI, section
426 S6) based on the limiting nutrient (N or P). During Stage III, acetate addition was ceased.
427 This was to assess process response to a sudden change, and to demonstrate that the
428 system requires wastewater with a specific COD/N/P ratio. State equations were
429 implemented in a fixed volume, completely mixed membrane bioreactor.

430 The results from the simulation were balanced over COD, N, P and C, and have been
431 included in the SI.

432 The Matlab function and run files, along with their supporting datasets, have been uploaded
433 to <http://espace.library.uq.edu.au/view/UQ:412280>.

434 3 Results

435 The sludge used for all the experiments came from a lab-scale PANMBR (Hülse et al.
436 2016b). Most of the microorganisms are related with *α-proteobacteria*, PPB accounting for
437 more than 70% of the total gene copies detected by the pyrosequencing technique. The
438 genus *Rhodobacter* ssp. is the most abundant, representing more than 60% of the
439 microbiota (Hülse et al. 2016b). The presence of photosynthetic organisms such as
440 microalgae and cyanobacteria accounts for less than 1% of total gene copies. Therefore, the
441 photo-biomass can be considered as PPB-dominated.

442 3.1 Growth Processes

443 Photoheterotrophy was assessed with VFAs and ethanol as substrate (Fig 2a). All
444 substrates were completely consumed during the experiment, and overall yields were similar
445 in all cases, with an average biomass yield of $1.13 \pm 0.21 \text{ mgCOD}_{\text{biomass}} \text{ mgCOD}^{-1}$. More
446 details are provided in the SI. As can be seen in Figure 2b, uptake rates of substrates
447 excluding acetate were similar, with a k_M of $1.3 \pm 0.1 \text{ (mgCOD mgCOD}^{-1} \text{ d}^{-1})$, and
448 undetectable K_S . Acetate had a significantly higher k_M ($2.4 \pm 0.2 \text{ mgCOD mgCOD}^{-1} \text{ d}^{-1}$) and
449 detectable, albeit low, K_S of $20 \pm 4 \text{ mgCOD L}^{-1}$. This essentially means that growth (uptake) is
450 faster on acetate, but with a lower affinity such that acetate uptake is faster at the beginning
451 of the batch, but slower at the end.

452 The analysis of chemoheterotrophic metabolism by PPB was conducted by using acetate
453 and ethanol as substrates in dark conditions (Figure 2c). PPB biomass was much less
454 effective in dark conditions compared with light conditions (biomass yield 0.5 vs 1.1

455 $\text{mgCOD}_{\text{biomass}} \text{ mgCOD}^{-1}$ in dark and light conditions, respectively). Biomass yield in dark
456 conditions is relatively high compared to typical values reported in literature for dark
457 fermentation and anaerobic oxidation processes, which are rarely greater than 0.2
458 $\text{mgCOD}_{\text{biomass}} \text{ mgCOD}^{-1}$ (Batstone et al. 2002). The occurrence of energy storage
459 (particularly poly-P) may have a significant role here due to batch operation (Liang et al.
460 2010). A continuous system may differ from this depending on the illumination cycle. One
461 with illumination in excess (operating with photo-heterotrophic growth only) is not influenced
462 by dark anaerobic fermentation. Where the illumination-non-illumination is separated by a
463 cycle on the order of days (or less), either in time or space, through reactor configuration or
464 a day-night illumination cycle the response is likely to be similar to the batch response here
465 (since the time scale is similar). However, where there are longer dark periods, stored
466 energy may be depleted, and this requires further investigation, since there is no supporting
467 literature. This may require inclusion of energy storage polymers, including poly-P, and
468 possibly PHA as well as consideration of methanogenic processes that occur when
469 photoheterotrophs can no longer effectively remove substrate.

470 The maximum uptake rate under dark conditions is approximately half that of
471 photoheterotrophy (Figure 2d), though with again, extremely low K_S values. While
472 chemotrophic growth is not dominant under photoheterotrophic conditions, it can be very
473 important to consider in reactor design (e.g., where there is insufficient light), and also for
474 balancing COD, C, N and P.

475 Analysis of photoautotrophy was done with NaHCO_3 as C source and Na_2S as electron
476 donor in 5-fold stoichiometric excess (see Table 2) (Figure 2e). The biomass had a yield of
477 $36,000 \text{ mgCOD}_{\text{biomass}} \text{ molC}^{-1}$ comparable to the value on acetate ($31,560 \text{ mgCOD}_{\text{biomass}}$
478 molC^{-1}). However, maximum uptake rate was far lower at $3.4 \pm 0.2 \times 10^{-6} \text{ molC mgCOD}^{-1} \text{ d}^{-1}$
479 (compared to $75 \pm 2 \times 10^{-6} \text{ molC mgCOD}^{-1} \text{ d}^{-1}$ on acetate) (Figure 2f). Photoautotrophy needs
480 to be considered for when there is an excess of bicarbonate and electrons from inorganic
481 sources in the wastewater. It is also important to consider photoautotrophy in order to close
482 mass balances. This case is particularly relevant in light deficiency, where fermentation and

483 anaerobic oxidation processes may become important and hence H_2 is available as a major
484 electron source for PPB.

485 Nutrient limitation experiments for N and P were used to determine saturation coefficients for
486 N and P. K_S values were extremely low such that the N and P regulation became a switch
487 function (data shown in SI). Biomass assimilated nutrients at a COD/N/P ratio of 100/7.1/1.8,
488 which is higher than conventional aerobic bacteria and much higher than other anaerobes
489 (Tchobanoglous et al., 2002). These values are in line with previous works (Hulsen et al.
490 2014). However, PPB were able to grow at a lower rate once the nutrients were completely
491 consumed (42% lower than in full nutrient conditions), likely due to fixation of headspace N_2
492 (Hunter et al. 2008) (inhibited in the presence of ammonium). Nitrogen fixation is completely
493 inhibited at any concentration of ammonium (threshold less than 20 mgN L^{-1}), and the
494 nitrogenase activation requires of a lag phase with no ammonium concentration to be active
495 again (section S5 of SI), likely due to activation of the transcription of nitrogenase genes
496 during static (not growing) conditions (Masepohl et al., 2002). Also, PPB can accumulate
497 polymers such as poly-P (Liang et al. 2010) as well as PHA (Melnicki et al. 2009), which can
498 be used in static growth mode. Since the model developed here is sustained on biomass
499 growth in presence of nitrogenase inhibiting ammonium, nutrient limitation for growth must
500 be included.

501 3.2 Endogenous processes – hydrolysis and decay

502 Hydrolysis and decay are considered as transversal first order biochemical processes in
503 most models (Batstone et al. 2006, Henze et al. 2000, Szilveszter et al. 2010). These could
504 be considered separately, since phototrophic growth can be restricted in the absence of
505 irradiance, and decay can be determined directly by measurement of phototrophic activity
506 following periods of irradiation without substrate. Figure 3 shows the time series of the SPA
507 values (on acetate) calculated for the PPB biomass during starvation. Biomass activity
508 reduced according to a first order model with decay coefficient of $0.09 \pm 0.02 \text{ d}^{-1}$. Hydrolysis
509 was assessed in dark conditions with substrate present, to avoid re-assimilation of products

510 by PPB. Therefore, hydrolysis products (organic C sources as COD, inorganic C as HCO_3^- ,
511 N as NH_4^+ and P as PO_4^{3-}) could be measured and were directly correlated with first order
512 kinetics of the hydrolytic process. Hydrolysis also followed a first order model with a
513 hydrolysis coefficient of $0.071 \pm 0.002 \text{ d}^{-1}$ (Fig 4). It should be noted that hydrolysis is
514 substrate specific, and is highly situation specific (Batstone et al. 2015), but that a value of
515 close to 0.1 d^{-1} is comparable with hydrolysis kinetics under anaerobic conditions, but much
516 lower than that for aerobic processes (Henze et al., 2000).

517 4 Discussion

518 4.1 Parameter values vs pure culture PPB

519 A full list of parameter values can be found in the SI, whereas Table 3 shows parameters
520 determined from the literature in comparison with those reported here. Parameters were
521 calculated on the basis that (i) protein composition of PPB is in all cases 60% of dry weight
522 (McKinlay and Harwood 2010), (ii) $1 \text{ g VSS} = 1.78 \text{ gCOD}$ and (iii) PPB biomass equation is
523 $\text{CH}_{1.8}\text{O}_{0.38}\text{N}_{0.18}$ (McKinlay and Harwood 2010).

524 In general, biomass yields calculated here are in line with values reported in the literature
525 (Table 3). The only exception is the biomass yield for autotrophic growth, where no relevant
526 values have been found and only indirect calculation can be performed. Wang et al. (1993)
527 reported biomass growth and CO_2 fixation in *Rhodobacter sphaeroides* and *Rhodospirillum*
528 *rubrum* using different electron sources (H_2 , thiosulfate, sulfide and malate) and the biomass
529 yield values extracted from their activities vary considerably with an average value of $84,000$
530 mgCOD molC^{-1} fixed. These values, however, did not consider re-fixation of CO_2 from
531 malate that may underestimate considerably real CO_2 usage for growth in the Calvin cycle
532 (McKinlay and Harwood 2011). Therefore the biomass yield differs from the value reported
533 here ($36,100 \pm 850 \text{ mgCOD molC}^{-1}$ fixed). The value determined during this study is

534 however very close to the theoretical maximum yield for carbon dioxide fixation of 39,840
535 mgCOD molC⁻¹, and as such, is a reasonable value.

536 However, specific uptake rates were substantially different to the literature values depending
537 on the growth mechanism, which may be due to use of pure cultures in contrast with mixed
538 cultures used in the present work. Generally, chemoheterotrophic parameters, pure cultures
539 have an activity close to two orders of magnitude higher than the mixed culture in this work.
540 This results in activities similar to those of typical fermentative bacteria. An example is found
541 in (Schultz and Weaver 1982) where the growth rates of *Rhodospirillum rubrum* and
542 *Rhodopseudomonas capsulata* were studied on several chemoheterotrophic substrates in
543 the dark. The authors used trimethylamine-N-oxide as accessory electron acceptor on
544 fructose, glucose and succinate, likely removing electron management as a major limitation.
545 Photoheterotrophic parameters also diverged depending on the substrate. While acetate
546 uptake rates were similar to the values reported here (Golomysova et al. 2010, McKinlay and
547 Harwood 2011), those obtained from other organics, such as malate (Gadhamshetty et al.
548 2008, Klein et al. 1991), lactate + malate (Obeid et al. 2009), or butyrate (McKinlay and
549 Harwood 2011) were almost one order of magnitude higher. These parameters were
550 obtained in hydrogen production studies. Under these situations, the substrate uptake is
551 optimized for biogenic H₂ by dislocating catabolism from anabolism due to excess of
552 electrons. This increases considerably the substrate uptake rate while minimizing yield
553 (Basak and Das 2007). In this work, the μ_{max} for photoheterotrophic metabolism was
554 calculated to be 1.54 d⁻¹, which corresponds to a doubling time of 0.45 d. It is similar to those
555 reported by McKinlay and Harwood (2011) (0.27-0.44 d), and generally aligns well with
556 purple phototrophic bacteria (Hunter et al. 2008). The use of pure cultures promotes specific
557 uptake rates to the detriment of substrate affinity. This leads to increased k_M and K_S
558 parameters, a typical behavior of r-strategist microorganisms (Dorodnikov et al. 2009).

559 Hydrolysis and decay rates are commonly substrate specific, with a decrease in rate as
560 redox decreases. In general, for a given material, the hydrolysis coefficient increases from

561 anaerobic to anoxic, and from anoxic to aerobic (Henze et al. 2000). The biomass decay and
562 hydrolysis constants found in literature were obtained in aerobic photoheterotrophic
563 processes (Huang et al. 1999, Huang et al. 2001). This explains considerably higher values
564 than those calculated here.

565 Compared with previous analyses, this study is focused on mixed culture photoheterotrophic
566 metabolism. The biomass seems to be a K-strategist which promotes substrate affinity over
567 uptake, a microbial strategy in low-strength systems as domestic wastewater with low
568 hydraulic retention times (less than 12 h). Such behavior is useful for out-competing other
569 fast-growing microorganisms. It is clearly effective when compared to the slow growing
570 methanogens, which are the only competitors for acetate under anaerobic conditions with
571 low concentrations of sulfate or oxidized metals (Dorodnikov et al. 2009). Indeed, PPB
572 microorganisms have been demonstrated to prevail and dominate in continuous PAnMBR
573 reactors treating real domestic wastewater without previous inoculation, both in mesophilic
574 (Hülßen et al. 2016b) as well as in psychrophilic (Hülßen et al. 2016a) conditions.

575 4.2 Model application

576 The model was tested in a realistic scenario, with influent profile generated using the BSM
577 influent generator (Gernaey et al. 2011). Detailed information about the simulations is
578 provided in the SI.

579 4.2.1 Fate of C, N and P

580 The model indicates different SCOD removal efficiencies for particular periods of operation.
581 In general, adaptation to seasonal periods of variable wastewater composition is rapid, as
582 can be shown in input values from Figures 5 and 6. For periods (I) and (III), which
583 correspond to no additional acetate in the system (average inlet SCOD of 293.1 ± 0.8
584 mgCOD L^{-1}), the mean SCOD removal efficiency is 81% (Figure 5a) The remaining SCOD in
585 the system can be mainly attributed to the presence of non-biodegradable SCOD,
586 accounting for 71% of the effluent SCOD. During period (II) acetate was added to agree with

587 the COD/N/P requirements for PPB. Average SCOD removal efficiency slightly increased up
588 to around 85% due to optimized COD/N/P conditions. As in the Stage I, the major part of the
589 remaining SCOD corresponded to soluble inerts. The model, however, is not able to
590 reproduce the PPB behavior under a high excess of inlet SCOD concentration since it is
591 based on assimilative mechanisms only and accumulation processes are not included, as
592 e.g. PHA or glycogen. The PPB biomass is able to accumulate these compounds (Brandl et
593 al. 1991, Melnicki et al. 2009), and so SCOD removal efficiencies are expected to be higher
594 and less dependent on nutrients in real cases (Hülßen et al. 2016a, Hülßen et al. 2016b). An
595 upgraded model including accumulative mechanisms is therefore needed for high COD:N
596 ratio wastewater. However, this model is suitable for normal DWW treatment operation,
597 where N and P are generally in excess.

598 Nutrient assimilation was directly linked with biomass growth. The optimum assimilative
599 COD/N/P relationship has been calculated to be 100/7.1/1.8 from batch experiments.
600 Therefore, periods with non-optimal ratios are expected to have higher effluent nutrient
601 concentrations. Under normal situation (periods (I) and (III)), with no additional acetate,
602 nutrients were not completely removed and ammonium and phosphate efficiencies were
603 45% and 56%, respectively (Figures 5b and 5c, respectively), averaging effluent
604 concentrations of 23 mgN L⁻¹ and 2.5 mgP L⁻¹, respectively. This justifies the need for extra
605 SCOD addition, as has been previously described experimentally (Hülßen et al. 2016b).
606 Phosphorus was almost completely removed during C and N sufficiency during period (II),
607 with removal efficiencies of 89% (effluent concentrations of 0.5 mgP L⁻¹). However, depletion
608 of P prevented a high N removal due to nutrient imbalance, and so N removal efficiencies
609 during these periods averaged 70%, averaging effluent concentrations of 11 mgN L⁻¹. Again,
610 accumulative mechanisms may have a key role here, as PPB are able to accumulate poly-P
611 (Liang et al. 2010). This mechanism is quite complex and has not been properly defined,
612 particularly in mixed cultures and on wastewater sources.

613 Production of biomass was related to PPB growth as well as input solids. Biomass
614 fractionation (X_{PB} , X_S and X_I) along the simulation period is depicted in Figure 6. When
615 acetate was not added, PPB biomass was produced at 26.9% of the total biomass in the
616 outlet (sludge line). Adding acetate increased this value up to 34.9% of total biomass.
617 Accumulation of X_S within the reactor is a direct consequence of low hydrolysis coefficient in
618 combination with short SRT. Additional substrate increased biomass concentration due to
619 assimilation of the remaining N and P. This also boosted the SRT, and decay was more
620 prominent, increasing X_S concentrations up to values above 1000 mgCOD L⁻¹ (see stage (II)
621 in Figure 6). Inerts fraction, however, was always below 32% of the total particulates
622 concentration, probably due to the slow hydrolysis rate. These results have an important
623 effect on energy distribution in the PRR platform since all energy balances are directly
624 related with the biomass management through anaerobic digestion, and the relative amount
625 of PPB will influence potential anaerobic degradability and biomass consistency. An
626 important aspect identified by this continuous analysis is that the biomass fraction X_{PB} is
627 always relatively small, even when applying a settler (compared with activated sludge
628 streams predicted by the ASM1). This is because the hydrolysis coefficient is very low (<0.1
629 d⁻¹) compared with the levels of >2 d⁻¹ typically applied in the ASM1, ASM2 and ASM2d
630 (Henze et al. 2000). This means that while growth rates are comparable to activated sludge,
631 hydrolysis rates are far lower, and hence metabolic activity is dominated by available soluble
632 substrate (and possibly N and P) rather than electron acceptor availability. In any case, there
633 will always be a large proportion of undegraded particulates, due to the slow hydrolysis
634 coefficient, and in a stable, solids dominated system, PPB sludge should be more analogous
635 to primary sludge rather than activated sludge, with both negative and positive
636 consequences.

637 pH followed some important general trends. During normal operation, it varied 6.5-7.5,
638 according to the VFA and bicarbonate uptake cycles. The overall pH was largely regulated
639 by the presence of bicarbonate, in opposition with inorganic nitrogen (S_{IN}). However, in

640 specific periods where the influent had bicarbonate limitations (approximately 2-3 weeks
641 every 6 months), where bicarbonate was completely depleted, pH could rise to 8.5-9 due to
642 the unbalanced presence of ammonia and cations. This was attenuated in the simulation
643 where cations were linked to bicarbonate, but was still a factor. We have seen batch tests
644 rise to pH 9 with no substantial impact on activity, and it is less evident, but obviously still
645 important in continuous operation. Very low pH levels (<6.0) never occurred, due to the lack
646 of nitrification. Likewise, at the ammonia levels present, despite the high pH, free ammonia
647 inhibition was never a risk, though it would be more important in industrial wastewaters.

648 Simulation of biomass behavior has implications on biomass production upon main line
649 biological treatment. There is a net increment of biomass production yield compared to
650 typical activated sludge processes. This could have an impact in energy recovery (through
651 biogas) but also in sludge waste disposal expenses, which can be partially counteracted by
652 downstream production of high value-added bioresources as proteins, prebiotics and
653 probiotics (Matassa et al. 2015) or bioplastics (Padovani et al. 2016), as well as energetic
654 resources as third generation liquid biofuels (Castro et al. 2016).

655

656 5 Conclusions

657 Anaerobic phototrophic growth in domestic wastewater treatment is fast, comparable to
658 activated sludge (in k_M values) with very low K_S values, indicating that purple phototrophic
659 bacteria behave as K strategist. However, hydrolysis is relatively slow ($\sim 0.1 \text{ d}^{-1}$), which
660 means that particulate substrates will not be degraded at short HRTs. The predominant
661 mechanism is photoheterotrophy, with autotrophy and chemotrophy generally slow. The
662 decay rate is relatively high, comparable to activated sludge under aerobic conditions. The
663 dynamics under continuous conditions indicate that biological processes are adaptable to
664 normal flow variations such that performance at a given mode is stable.

665 The model has the following limitations:

- 666 (i) The model is only valid for anaerobic conditions, and hydrogen production for
667 redox balancing is assumed to be inhibited, so this model cannot be implemented
668 for hydrogen production systems as it is.
- 669 (ii) Poly-P and other polymers accumulation is not included due to a lack of
670 foundational research. Also, nitrogen fixation is not included since it is assumed
671 to be inhibited by ammonium.

672 A key priority for future research should be inclusion of poly-P and PHA accumulation as well
673 as N_2 fixation and side H_2 production, as these processes (poly-P without carbon, PHA
674 without oxidation or organics, and N_2/H_2 production) are unique to photoanaerobic
675 organisms. The topic of infrared light delivery has not been addressed in detail in this model,
676 and is generally assumed to be in excess (i.e., not limiting catabolic rate, such that there is
677 no mixed photo-dark fermentation (mixotrophic growth). This could be incorporated by
678 limiting light to enable mixotrophic growth through the existing switch function that considers
679 also spatial separation to dark zones, but as stated above, further work is required to
680 consider accumulation and depletion of storage compounds. This requires a very different
681 approach to (for example, Algae) (reviewed in Béchet et al. 2013) where a more complex
682 model is commonly applied: (considering separately excited, resting, inhibited differential
683 states). We have kept PPB biomass as a single state, with different processes acting on it,
684 which are in turn linked to the presence or absence of irradiance, which would enable more
685 simple extension to energy storage and depletion. This would enable more precise
686 determination of the switch between stored dark heterotrophic growth and methanogenesis.

687 6 ACKNOWLEDGEMENTS

688 This work was jointly funded by the Smart Water Fund (project 10OS-023) and the CRC for
689 Water Sensitive Cities (project C2.1). Thanks are given to Prof. James B. McKinlay for his
690 kind discussion on PPB metabolism.

691 **7 REFERENCES**

692 APHA., 1998. Standard Methods for the Examination of Water and Wastewater. 20th ed.

693 American Public Health Association, Washington, DC, USA.

694 Basak, N. and Das, D., 2007. The prospect of purple non-sulfur (PNS) photosynthetic

695 bacteria for hydrogen production: the present state of the art. *World Journal of Microbiology*

696 and *Biotechnology* 23(1), 31-42.

697 Batstone, D.J., Amerlinck, Y., Ekama, G., Goel, R., Grau, P., Johnson, B., Kaya, I., Steyer,

698 J.P., Tait, S., Takaács, I., Vanrolleghem, P.A., Brouckaert, C.J. and Volcke, E., 2012.

699 Towards a generalized physicochemical framework. *Water Science and Technology* 66(6),

700 1147-1161.

701 Batstone, D.J., Keller, J., Angelidaki, I., Kalyuzhnyi, S., Pavlostathis, S., Rozzi, A., Sanders,

702 W., Siegrist, H. and Vavilin, V., 2002. The IWA Anaerobic Digestion Model No 1(ADM 1).

703 *Water Science and Technology* 45(10), 65-73.

704 Batstone, D.J., Keller, J. and Steyer, J., 2006. A review of ADM 1 extensions, applications,

705 and analysis: 2002-2005. *Water Science and Technology* 54(4), 1-10.

706 Batstone, D.J., Pind, P.F. and Angelidaki, I., 2003. Kinetics of thermophilic, anaerobic

707 oxidation of straight and branched chain butyrate and valerate. *Biotechnology and*

708 *Bioengineering* 84(2), 195-204.

709 Batstone, D.J., Puyol, D., Flores-Alsina, X. and Rodríguez, J., 2015. Mathematical modelling

710 of anaerobic digestion processes: applications and future needs. *Reviews in Environmental*

711 *Science and Bio/Technology* 14(4), 595-613.

- 712 Brandl, H., Gross, R.A., Lenz, R.W., Lloyd, R. and Fuller, R.C., 1991. The accumulation of
713 poly(3-hydroxyalkanoates) in *Rhodobacter sphaeroides*. Archives of Microbiology 155(4),
714 337-340.
- 715 Béchet, Q., Shilton, A., & Guieysse, B., 2013. Modeling the effects of light and temperature
716 on algae growth: State of the art and critical assessment for productivity prediction during
717 outdoor cultivation. Biotechnology Advances, 31(8), 1648–1663
- 718 Castro, A.R., Rocha, I., Alves, M.M. and Pereira, M.A., 2016. *Rhodococcus opacus* B4: a
719 promising bacterium for production of biofuels and biobased chemicals. AMB Express 6:35.
- 720 Chen, Y., Cheng, J.J. and Creamer, K.S., 2008. Inhibition of anaerobic digestion process: A
721 review. Bioresource Technology 99(10), 4044-4064.
- 722 Copp, J.B., Jeppsson, U., Rosen, C., 2003. Towards an ASM1 – ADM1 state variable
723 interface for plant-wide wastewater treatment modeling. In: Proceedings of the 76th Annual
724 WEF Conference and Exposition (WEFTEC). Oct. 11–15, Los Angeles, USA.
- 725 Dorodnikov, M., Blagodatskaya, E., Blagodatsky, S., Fangmeier, A. and Kuzyakov, Y., 2009.
726 Stimulation of r- vs. K-selected microorganisms by elevated atmospheric CO₂ depends on
727 soil aggregate size: Research article. FEMS Microbiology Ecology 69(1), 43-52.
- 728 Eroglu, I., 2008. Hydrogen production by *Rhodobacter sphaeroides* O.U.001 in a flat plate
729 solar bioreactor. International Journal of Hydrogen Energy 33(2), 531-541.
- 730 Fang, H.H.P., Liu, H. and Zhang, T., 2005. Phototrophic hydrogen production from acetate
731 and butyrate in wastewater. International Journal of Hydrogen Energy 30(7), 785-793.
- 732 Finneran, K.T., Johnsen, C.V. and Lovley, D.R., 2003. *Rhodoferrax ferrireducens* sp. nov., a
733 psychrotolerant, facultatively anaerobic bacterium that oxidizes acetate with the reduction of
734 Fe(III). International Journal of Systematic and Evolutionary Microbiology 53(3), 669-673.

- 735 Gadhamshetty, V., Sukumaran, A., Nirmalakhandan, N. and Theinmyint, M., 2008.
736 Photofermentation of malate for biohydrogen production— A modeling approach.
737 International Journal of Hydrogen Energy 33(9), 2138-2146.
- 738 Gernaey, K.V., Flores-Alsina, X., Rosen, C., Benedetti, L. and Jeppsson, U., 2011. Dynamic
739 influent pollutant disturbance scenario generation using a phenomenological modelling
740 approach. Environmental Modelling & Software 26(11), 1255-1267.
- 741 Golomysova, A., Gomelsky, M. and Ivanov, P.S., 2010. Flux balance analysis of
742 photoheterotrophic growth of purple nonsulfur bacteria relevant to biohydrogen production.
743 International Journal of Hydrogen Energy 35(23), 12751-12760.
- 744 Gordon, G.C. and McKinlay, J.B., 2014. Calvin cycle mutants of photoheterotrophic purple
745 nonsulfur bacteria fail to grow due to an electron imbalance rather than toxic metabolite
746 accumulation. Journal of Bacteriology 196(6), 1231-1237.
- 747 Henze, M., Gujer, W., Mino, T. and Van Loosdrecht, M., 2000. Activated sludge models
748 ASM1, ASM2, ASM2d and ASM3. Vol. 9. IWA Publishing, UK.
- 749 Hiraishi, A., Yanase, A. and Kitamura, H., 1991. Polyphosphate accumulation by
750 *Rhodobacter sphaeroides* grown under different environmental conditions with special
751 emphasis on the effect of external phosphate concentrations. Bulletin of Japanese Society of
752 Microbial Ecology 6(1), 25-32.
- 753 Huang, J.S., Jih, C.G. and Sung, T.J., 1999. Performance enhancement of suspended-
754 growth reactors with phototrophs. Journal of Environmental Engineering 125(6), 501-507.
- 755 Huang, J.S., Wu, C.S., Jih, C.G. and Chen, C.T., 2001. Effect of addition of *Rhodobacter* sp.
756 to activated-sludge reactors treating piggery wastewater. Water Research 35(16), 3867-
757 3875.

- 758 Hülsen, T., Barry, E.M., Lu, Y., Puyol, D. and Batstone, D.J., 2016a. Low temperature
759 treatment of domestic wastewater by purple phototrophic bacteria: Performance, activity,
760 and community. *Water Research* 100, 537-545.
- 761 Hülsen, T., Barry, E.M., Lu, Y., Puyol, D., Keller, J. and Batstone, D.J., 2016b. Domestic
762 wastewater treatment with purple phototrophic bacteria using a novel continuous photo
763 anaerobic membrane bioreactor. *Water Research* 100, 486-495.
- 764 Hülsen, T., Batstone, D.J. and Keller, J., 2014. Phototrophic bacteria for nutrient recovery
765 from domestic wastewater. *Water Research* 50, 18-26.
- 766 Hunter, C.N., Daldal, F., Thurnauer, M.C. and Beatty, J.T., 2008. *The Purple Phototrophic*
767 *Bacteria*. Springer, The Netherlands.
- 768 Jetten, M.S.M., Horn, S.J. and van Loosdrecht, M.C.M., 1997. Towards a more sustainable
769 municipal wastewater treatment system. *Water Science and Technology* 35(9), 171-180.
- 770 Kantachote, D., Torpee, S. and Umsakul, K., 2005. The potential use of anoxygenic
771 phototrophic bacteria for treating latex rubber sheet wastewater. *Electronic Journal of*
772 *Biotechnology* 8(3), 314-323.
- 773 Kim, M.K., Choi, K.-M., Yin, C.-R., Lee, K.-Y., Im, W.-T., Lim, J.H. and Lee, S.-T., 2004.
774 Odorous swine wastewater treatment by purple non-sulfur bacteria, *Rhodopseudomonas*
775 *palustris*, isolated from eutrophicated ponds. *Biotechnology Letters* 26(10), 819-822.
- 776 Klamt, S., Schuster, S. and Gilles, E.D., 2002. Calculability analysis in underdetermined
777 metabolic networks illustrated by a model of the central metabolism in purple nonsulfur
778 bacteria. *Biotechnology and Bioengineering* 77(7), 734-751.
- 779 Klein, G., Klipp, W., Jahn, A., Steinborn, B. and Oelze, J., 1991. The relationship of biomass,
780 polysaccharide and H₂ formation in the wild-type and nifA/nifB mutants of *Rhodobacter*
781 *capsulatus*. *Archives of Microbiology* 155(5), 477-482.

- 782 Lee, H.-S., Vermaas, W.F. and Rittmann, B.E., 2010. Biological hydrogen production:
783 prospects and challenges. *Trends in Biotechnology* 28(5), 262-271.
- 784 Liang, C.-M., Hung, C.-H., Hsu, S.-C. and Yeh, I.-C., 2010. Purple nonsulfur bacteria
785 diversity in activated sludge and its potential phosphorus-accumulating ability under different
786 cultivation conditions. *Applied Microbiology and Biotechnology* 86(2), 709-719.
- 787 Madigan, M.T. and Gest, H., 1978. Growth of a photosynthetic bacterium anaerobically in
788 darkness, supported by "oxidant-dependent" sugar fermentation. *Archives of Microbiology*
789 117(2), 119-122.
- 790 Masepohl, B., Drepper, T., Paschen, A., Groß, S., Pawlowski, A., Raabe, K., ... & Klipp, W.,
791 2002. Regulation of nitrogen fixation in the phototrophic purple bacterium *Rhodobacter*
792 *capsulatus*. *Journal of molecular microbiology and biotechnology* 4(3), 243-248.
- 793 Matassa, S., Batstone, D.J., Hülsen, T., Schnoor, J. and Verstraete, W., 2015. Can direct
794 conversion of used nitrogen to new feed and protein help feed the world? *Environmental*
795 *Science and Technology* 49(9), 5247-5254.
- 796 McKinlay, J.B. and Harwood, C.S., 2010. Carbon dioxide fixation as a central redox cofactor
797 recycling mechanism in bacteria. *Proceedings of the National Academy of Sciences of the*
798 *United States of America* 107(26), 11669-11675.
- 799 McKinlay, J.B. and Harwood, C.S., 2011. Calvin cycle flux, pathway constraints, and
800 substrate oxidation state together determine the H₂ biofuel yield in photoheterotrophic
801 bacteria. *MBio* 2(2), e00323-00310.
- 802 Melnicki, M.R., Eroglu, E. and Melis, A., 2009. Changes in hydrogen production and polymer
803 accumulation upon sulfur-deprivation in purple photosynthetic bacteria. *International Journal*
804 *of Hydrogen Energy* 34(15), 6157-6170.

- 805 Muñoz, R. and Guieysse, B., 2006. Algal–bacterial processes for the treatment of hazardous
806 contaminants: A review. *Water Research* 40(15), 2799-2815.
- 807 Obeid, J., Magnin, J., Flaus, J., Adrot, O., Willison, J. and Zlatev, R., 2009. Modelling of
808 hydrogen production in batch cultures of the photosynthetic bacterium *Rhodobacter*
809 *capsulatus*. *International Journal of Hydrogen Energy* 34(1), 180-185.
- 810 Overmann, J. and Garcia-Pichel, F., 1998. The phototrophic way of life: The Prokaryotes: an
811 evolving electronic resource for the microbiological community. M. Dworkin, New York.
812 Springer, The Netherlands.
- 813 Padovani, G., Carlozzi, P., Seggiani, M., Cinelli, P., Vitolo, S. and Lazzeri, A., 2016. PHB-
814 rich biomass and BioH₂ production by means of photosynthetic microorganisms. *Chemical*
815 *Engineering Transactions* 49, 55-60.
- 816 Patton, C.J. and Truitt, E.P., 1992. *Methods of Analysis by the US Geological Survey*
817 *National Water Quality Laboratory: Determination of the Total Phosphorus by a Kjeldahl*
818 *Digestion Method and an Automated Colorimetric Finish that Includes Dialysis, Open-File*
819 *Report 92-146. US Geological Survey, USA.*
- 820 Rodionov, Y.V., Lebedeva, N.V. and Kondratieva, E.N., 1986. Ammonia inhibition of
821 nitrogenase activity in purple and green bacteria. *Archives of Microbiology* 143(4), 345-347.
- 822 Sarles, L.S. and Tabita, F.R., 1983. Derepression of the synthesis of D-ribulose 1, 5-
823 bisphosphate carboxylase/oxygenase from *Rhodospirillum rubrum*. *Journal of Bacteriology*
824 153(1), 458-464.
- 825 Schultz, J. and Weaver, P., 1982. Fermentation and anaerobic respiration by *Rhodospirillum*
826 *rubrum* and *Rhodopseudomonas capsulata*. *Journal of Bacteriology* 149(1), 181-190.

- 827 Seitz, H.J., Schink, B., Pfennig, N. and Conrad, R., 1990. Energetics of syntrophic ethanol
828 oxidation in defined chemostat cocultures - 1. Energy requirement for H₂ production and H₂
829 oxidation. Archives of Microbiology 155(1), 82-88.
- 830 Szilveszter, S., Ráduly, B., Ábrahám, B., Lányi, S. and Niculae, D.R., 2010. Mathematical
831 models for domestic biological wastewater treatment process. Environmental Engineering
832 and Management Journal 9(5), 629-636.
- 833 Tait, S., Tamis, J., Edgerton, B. and Batstone, D.J., 2009. Anaerobic digestion of spent
834 bedding from deep litter piggery housing. Bioresource Technology 100(7), 2210-2218.
- 835 Tao, Y., He, Y., Wu, Y., Liu, F., Li, X., Zong, W. and Zhou, Z., 2008. Characteristics of a new
836 photosynthetic bacterial strain for hydrogen production and its application in wastewater
837 treatment. International Journal of Hydrogen Energy 33(3), 963-973.
- 838 Tchobanoglous, G., Stensel, H.D., Tsuchihashi, R. and Burton, F.L. 2002. Wastewater
839 engineering: treatment and reuse, Metcalf and Eddy Inc, 4th ed. McGraw-Hill Education,
840 New York, NY, USA.
- 841 Uyar, B., Eroglu, I., Yücel, M., Gündüz, U. and Türker, L., 2007. Effect of light intensity,
842 wavelength and illumination protocol on hydrogen production in photobioreactors.
843 International Journal of Hydrogen Energy 32(18), 4670-4677.
- 844 Wang, X., Modak, H.V. and Tabita, F.R., 1993. Photolithoautotrophic growth and control of
845 CO₂ fixation in *Rhodobacter sphaeroides* and *Rhodospirillum rubrum* in the absence of
846 ribulose bisphosphate carboxylase-oxygenase. Journal of Bacteriology 175(21), 7109-7114.
- 847 Yetis, M., Gündüz, U., Eroglu, I., Yücel, M. and Türker, L., 2000. Photoproduction of
848 hydrogen from sugar refinery wastewater by *Rhodobacter sphaeroides* OU 001. International
849 Journal of Hydrogen Energy 25(11), 1035-1041.

850 Zhu, H., Suzuki, T., Tsygankov, A.A., Asada, Y. and Miyake, J., 1999. Hydrogen production
851 from tofu wastewater by *Rhodobacter sphaeroides* immobilized in agar gels. International
852 Journal of Hydrogen Energy 24(4), 305-310.

853

ACCEPTED MANUSCRIPT

854 TABLES

855 **Table 1.** Petersen matrix of the PAM-1 model for domestic wastewater treatment by PPB.

Component (C) →		<i>i</i>	1	2	3	4	5	6	7	8	9	10
<i>j</i>	Process↓	S_S	S_{ac}	S_{IC}	S_{h2}	S_{IN}	S_{IP}	S_I	X_{PB}	X_S	X_I	
1	Hydrolysis/fermentation	$f_{ss,xs}$	$f_{Sac,xs}$	$f_{IC,xs}$	$f_{h2,xs}$	$f_{IN,xs}$	$f_{IP,xs}$	$f_{si,xs}$	0	-1	$f_{xi,xs}$	
2	Acetate uptake	0	-1	$f_{IC,ph,ac}$	0	$-f_{N,B}Y_{PB,ph}$	$-f_{P,B}Y_{PB,ph}$	0	$Y_{PB,ph}$	0	0	
3	Photoheterotrophic uptake	-1	0	$-f_{IC,ph,ss}$	0	$-f_{N,B}Y_{PB,ph}$	$-f_{P,B}Y_{PB,ph}$	0	$Y_{PB,ph}$	0	0	
4	Chemoheterotrophic uptake	-1	(1- $Y_{PB,ch}$) $f_{ac,ch}$	0	(1- $Y_{PB,ch}$) $f_{h2,ch}$	$-f_{N,B}Y_{PB,ch}$	$-f_{P,B}Y_{PB,ch}$	0	$Y_{PB,ch}$	0	0	
5	Autotrophic uptake	0	0	$-f_{IC,a}$	$-f_{h2,a}$	$-f_{N,B}Y_{PB,a}$	$-f_{P,B}Y_{PB,a}$	0	$Y_{PB,a}$	0	0	
6	Decay of XPB	0	0	$-\sum_{i=8-9} C_i$ $\times f_{C,i}$	0	$-\sum_{i=8-9} C_i$ $\times f_{N,i}$	$-\sum_{i=8-9} C_i$ $\times f_{P,i}$	0	-1	1	0	

Limiting factors:

Competitive inhibition: $I_{C_S} = \frac{S_{ac}}{S_{ac} + S_S}$ $I_{C_{ac}} = \frac{S_S}{S_S + S_{ac}}$

N: $I_{IN} = \left(\frac{S_{IN}}{K_{S,IN} + S_{IN}} \right)$ P: $I_{IP} = \left(\frac{S_{IP}}{K_{S,IP} + S_{IP}} \right)$ Free Ammonia: $I_{FA} = \left(\frac{K_{I,FA}}{K_{I,FA} + S_{NH_3}} \right)$ Light: $I_E = \left(\frac{S_E}{K_{S,E} + S_E} \right)$

856

857 **Table 2:** Batch conditions of the different metabolic tests.

Mechanism	Medium	Buffer system [*]	COD/N/P (C/N/P) ^{***}	C source (mgCOD L ⁻¹) ¹⁾	Electron donor (mg L ⁻¹)	Electron acceptor	Positive control	Negative control
Photoheterotrophy	Ormerod	HEPES	100/10/2	Acetate (130), propionate, butyrate, ethanol (100)	Organic	CO ₂	Adding 1 g NaHCO ₃	-
Nitrogen limitation	Ormerod	HEPES	100/1.4/2	Acetate (130)	Organic	CO ₂	No N limitation	-
Phosphorus limitation	Ormerod	HEPES	100/10/0.15	Acetate (130)	Organic	CO ₂	No P limitation	-
Photoautotrophy	Ormerod	Phosphate	(100/20/∞)	NaHCO ₃ (0.012) ^{**}	Na ₂ S (300)	CO ₂	-	No Na ₂ S
Chemoheterotrophy (dark)	Ormerod	HEPES	100/10/2	Ethanol (60), Acetate (130)	Organic	Acetate	With light	-
Inhibition of H ₂ production	DWW	-	100/12/4	DWW (278)	Organic	CO ₂	-	Acetate (600)
	Ormerod	Phosphate	100/15/∞	Acetate (600)	Organic	CO ₂	-	N limitation (1/10)

858 ^{*} Buffer systems: HEPES (5.9 g L⁻¹), Phosphate (0.9 g K₂HPO₄ + 0.66 g KH₂PO₄). ^{**} molC L⁻¹ ^{***} ∞ means in high excess due to
859 buffering

860

861 **Table 3:** Comparison of estimated parameters with those reported in the literature.

Parameter	Units	Estimated values	Literature values	Refs.
$k_{M,ac}$	mgCOD mgCOD ⁻¹ d ⁻¹	2.4	1.5 (0.5), n=2	1
$k_{M,ph}$	mgCOD mgCOD ⁻¹ d ⁻¹	1.4	11 (13), n=12	2
$k_{M,ch}$	mgCOD mgCOD ⁻¹ d ⁻¹	0.074	5 (4), n=8	3
$k_{M,ic}$	molC mgCOD ⁻¹ d ⁻¹	$3.4 \cdot 10^{-6}$	$2.5 \cdot 10^{-5}$ ($1.7 \cdot 10^{-5}$), n= 9	4
$K_{S,s}$	mgCOD L ⁻¹	0.5	4,333 (6,036), n=2	5
$Y_{PB,ph}$	mgCOD mgCOD ⁻¹	1.1	0.78 (0.37), n=17	6
$Y_{PB,ch}$	mgCOD mgCOD ⁻¹	0.5	0.23 (0.12), n= 8	7
$Y_{PB,a}$	mgCOD molC ⁻¹	36,100	132,000 (84,000), n=4	8
k_{hyd}	d ⁻¹	0.07	0.27 (0.06), n=2	9
k_{dec}	d ⁻¹	0.09	0.2 (0.02), n=2	10

862 ¹ (Golomysova et al. 2010, McKinlay and Harwood 2011), ² (Gadhamshetty et al. 2008,
863 Golomysova et al. 2010, Klein et al. 1991, McKinlay and Harwood 2011, Obeid et al. 2009), ³
864 (Madigan and Gest 1978, Schultz and Weaver 1982), ⁴ (Sarles and Tabita 1983, Wang et al.
865 1993), ⁵ (Gadhamshetty et al. 2008, Obeid et al. 2009), ⁶ (Gadhamshetty et al. 2008, Klamt
866 et al. 2002, Klein et al. 1991, McKinlay and Harwood 2011, Obeid et al. 2009, Schultz and
867 Weaver 1982), ⁷ (Madigan and Gest 1978, Schultz and Weaver 1982), ⁸ (Wang et al. 1993),
868 ⁹ (Huang et al. 1999, Huang et al. 2001), ¹⁰ (Huang et al. 1999, Huang et al. 2001)

869

870 **FIGURE CAPTIONS**

871

872 **Figure 1:** Schematic summary of PPB metabolism under domestic wastewater treatment.

873 Key: N₂ase: Nitrogenase complex. TCA-c: Tri-carboxylic acid cycle. DF: Dark fermentation.

874 VFA: volatile fatty acids. e⁻: electrons. Dash: electron cycles. Dot: proton pumps. *: Model

875 components.

876 **Figure 2:** Experimental (symbols) and modelled (lines) time course of substrates uptake (left)

877 and parameters determination including 95% confidence intervals and confidence regions

878 (right) of PPB metabolism in photoheterotrophy (a), chemoheterotrophy (b) and

879 photoautotrophy (c) growth modes.

880 **Figure 3:** Mechanism of decay rate. Time course of specific phototrophic activity of PPB

881 subjected to starvation under full illumination.

882 **Figure 4:** Time course of released products upon starvation in dark conditions

883 demonstrating hydrolysis: soluble organic compounds but acetate (squares), acetate

884 (diamonds), hydrogen (triangles), TIC (pluses), NH₄⁺-N (circles) and PO₄³⁻-P (crosses).

885 **Figure 5:** Influent (continuous line) and effluent concentrations (dash line) over time for

886 PAnMBR simulation for SCOD (a), ammonium (b) and phosphate (c) upon primary settling.

887 Different operational periods are indicated as vertical shades separators.

888 **Figure 6:** Biomass fractionation including active phototrophic bacteria (dash line),

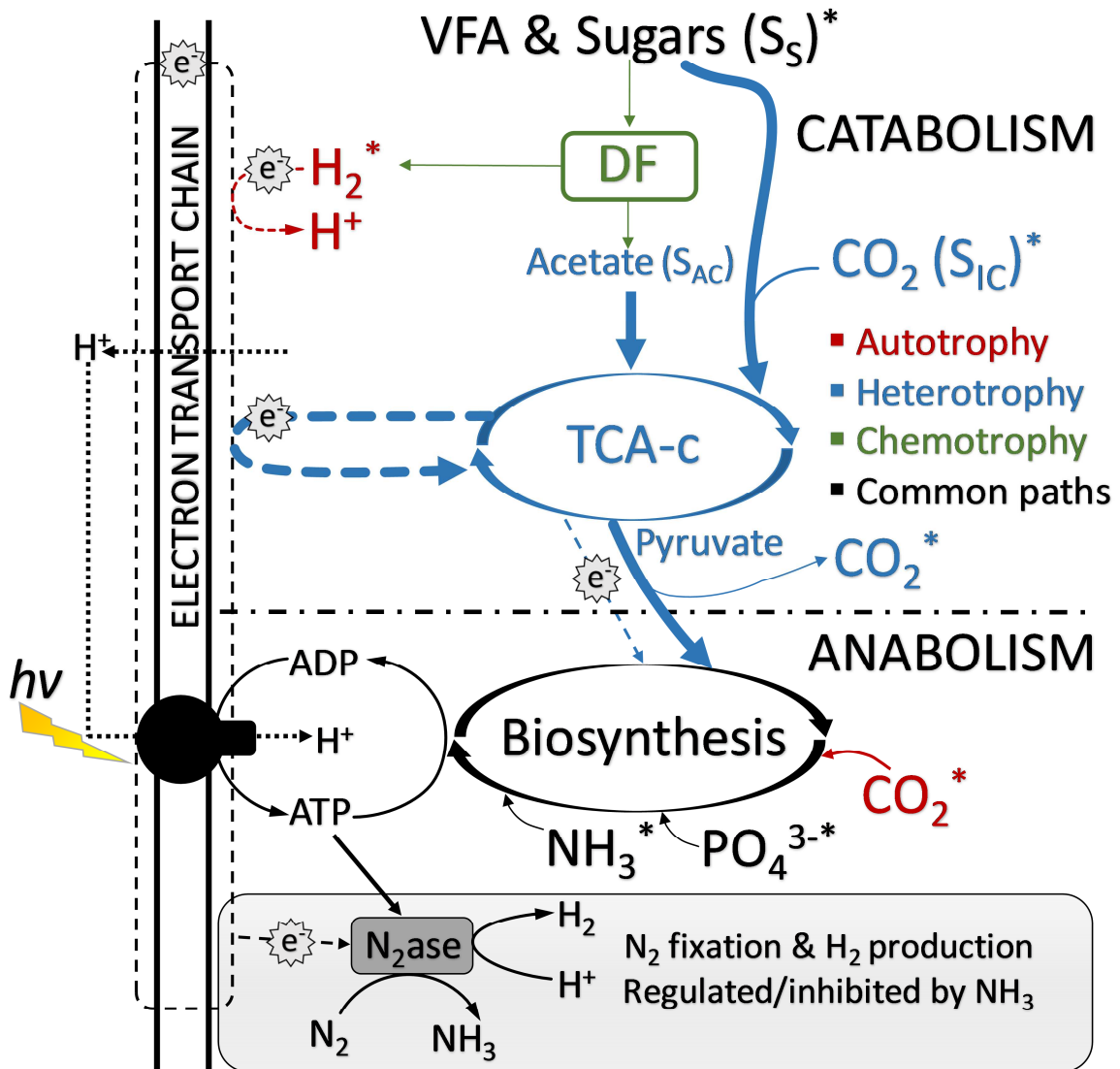
889 biodegradable particulate biomass (continuous line) and inert particulate (dot lines) over time

890 for the PAnMBR continuous simulation. Different operational periods are indicated as vertical

891 shades separators.

892

893 FIGURE 1

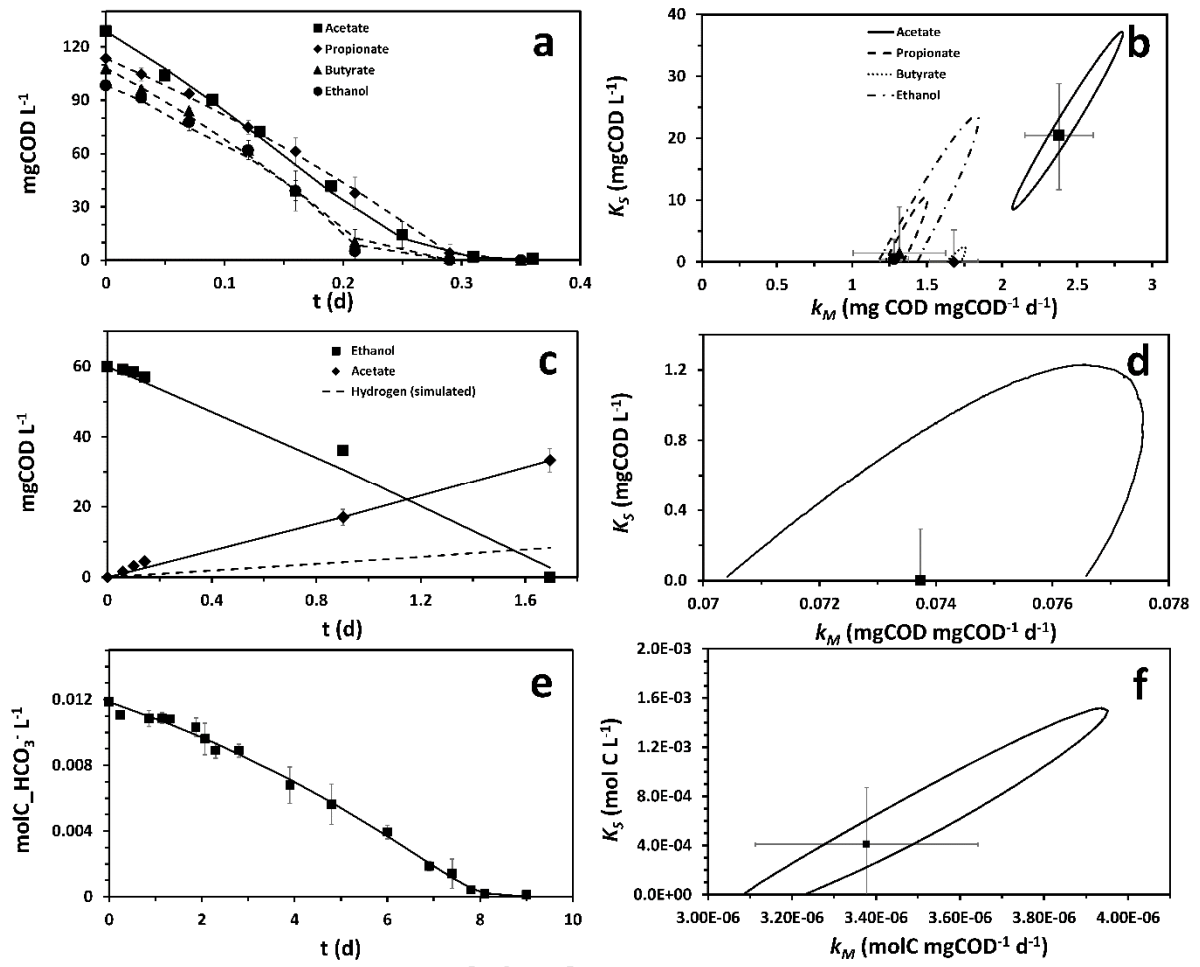


894

895

896 **FIGURE 2**

897

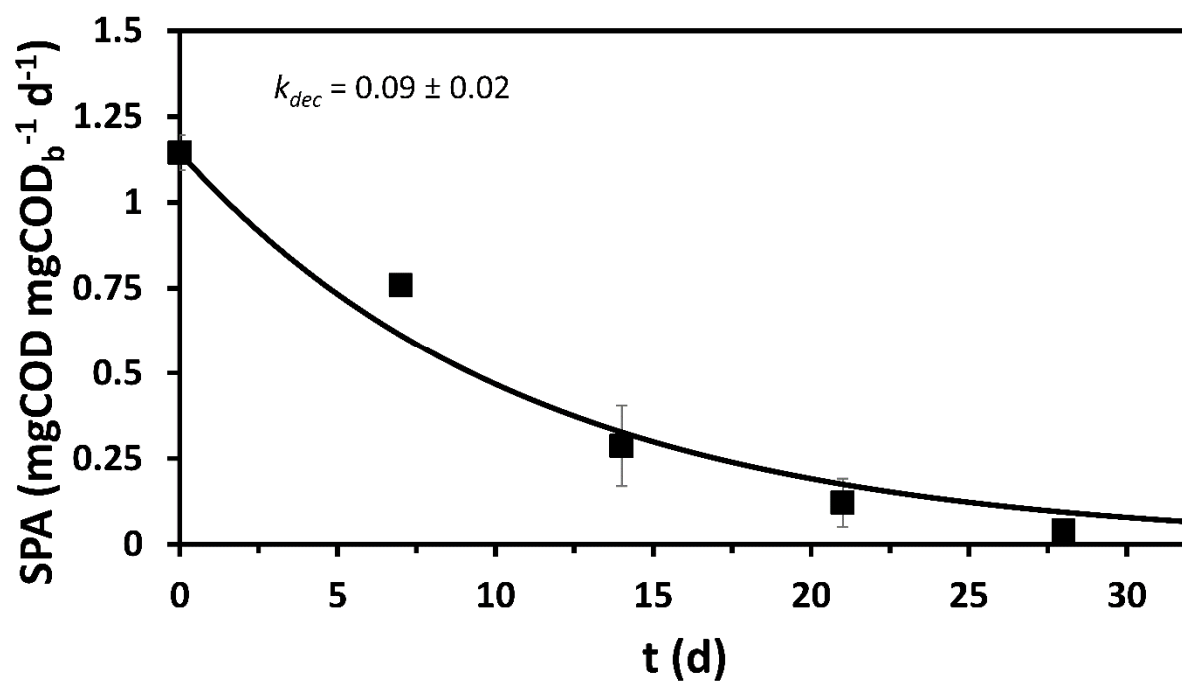


898

899

900 **FIGURE 3**

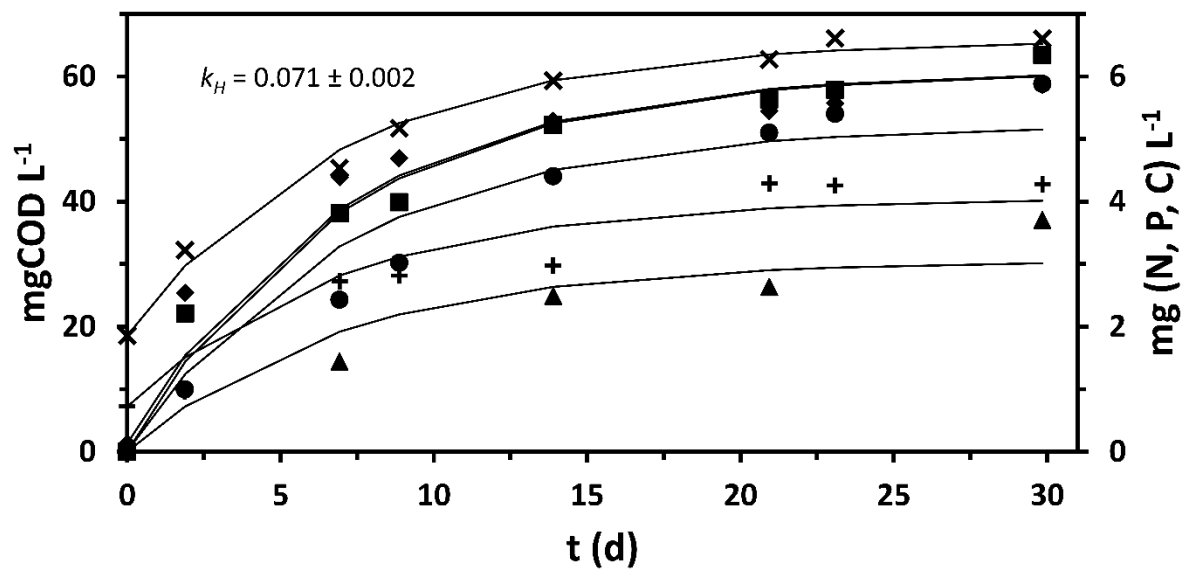
901



902

903

904 FIGURE 4

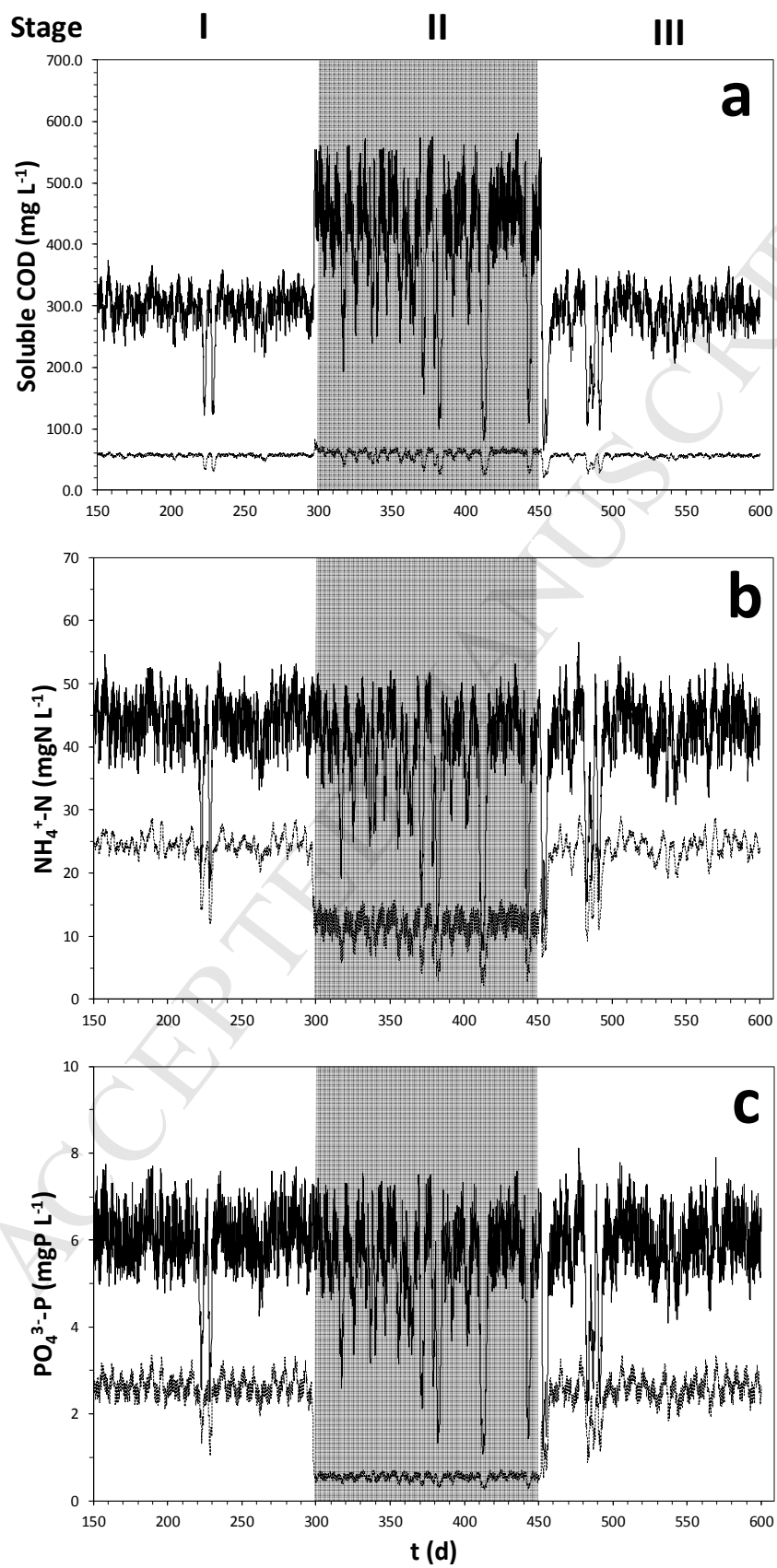


905

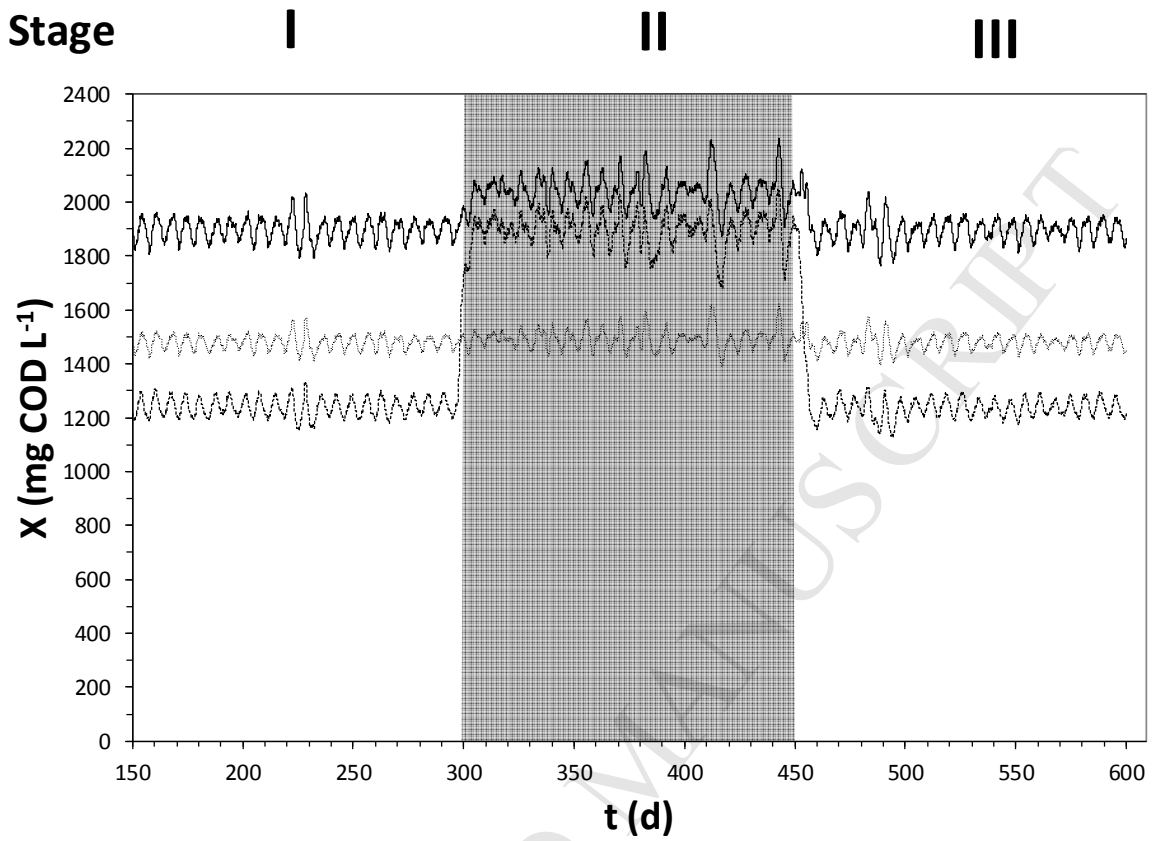
906

ACCEPTED MANUSCRIPT

907 FIGURE 5



908

909 **FIGURE 6**

910

911

912

1 **HIGHLIGHTS**

- 2 - A mechanistic model for anaerobic phototrophs has been developed: PAnM
- 3 - The model includes organic C and H₂ (as COD) and inorganic C, N and P.
- 4 - Microbial processes based on PPB metabolism were identified through dedicated
5 experiments.
- 6 - Kinetic and stoichiometric parameters were determined in batch tests.
- 7 - Model was tested by simulating the process in a photo-anaerobic MBR

ACCEPTED MANUSCRIPT